RSC Advances

PAPER

View Article Online
View Journal | View Issue

Cite this: *RSC Adv.*, 2018, **8**, 35819

Concentration dependence of As_2S_3 chalcogenide glass cluster size in amine solution

Nikita S. Dutta and Craig B. Arnold*

Received 12th September 2018
Accepted 15th October 2018

DOI: 10.1039/c8ra07610c

rsc.li/rsc-advances

Solution processing chalcogenide glasses is a common and effective first step in optoelectronic device fabrication. Arsenic(III) sulfide (As_2S_3) is believed to take on a nanoscale cluster structure in *n*-propylamine and *n*-butylamine, which affects the morphology and properties of the deposited material; however, the size of these clusters and the mechanism of size determination are poorly understood. We combine experimental and analytical techniques to investigate As_2S_3 cluster size in *n*-propylamine and its dependence on solution concentration. We find that the cluster size increases with concentration and show that this trend is consistent across independent experimental techniques. We then explain these results by proposing a simplified dissolution mechanism and deriving cluster size through a free energy argument. Our findings enable informed control of chalcogenide glass cluster size during solution processing and improved property control in optoelectronic device fabrication.

1 Introduction

Chalcogenide glasses (ChGs) have long been of interest for optoelectronic applications. Their transmission in the mid-infrared (mid-IR) enables waveguides and optical fibers for chemical sensing, thermal imaging, and medicine.[1–4] Their high optical nonlinearities and photoinduced phenomenon like photoexpansion, photodarkening, and photocrystallization give rise to applications in optical switching and information storage.[5–9] Doping with metallic nanoparticles can be used to enhance these desirable traits.[10,11]

A variety of processing methods are available for ChGs; among these, solution processing is popular for its flexibility.[12] The glasses dissolve in organic solvents and can then be doped, spin coated, or even inkjet printed with relative ease.[12–15] Previous research has shown numerous successful applications, including molded mid-IR waveguides, drop-cast photonic crystals, and optical fibers with a nonlinearity-enhancing ChG coating.[16–19]

The pioneering work on ChG solutions was done by Chern *et al.* using As_2S_3 in *n*-propylamine and *n*-butylamine as test systems.[20] Nuclear magnetic resonance showed the presence of an amine salt—evidence of a solvent–solute reaction—while UV absorption remained similar to that of the bulk glass. They hypothesized that As_2S_3 took on a molecular structure in solution, consisting of nano-sized As_2S_3 clusters within an amine salt shell. Years later, Kohoutek *et al.* used results from dynamic light scattering (DLS) to claim that the size of the clusters increased with concentration.[21]

Cluster size is an important attribute of solutions as ChGs, like many materials, have shown size-dependent optical properties at the nanoscale, and As_2S_3 solutions are a useful system since they are technologically relevant with a structure mirrored by solutions of other ChGs and even some crystals.[22–24] Despite this, the proposed concentration dependence of As_2S_3 cluster size has not been verified by independent methods and the processes underlying size determination have not been explained. This limits the improvement of ChG solution processing to inefficient reverse engineering.

In this work, we address this gap in knowledge by fully exploring the size of As_2S_3 clusters in *n*-propylamine. By combining DLS with viscosity measurements and cryo-transmission electron microscopy (cryo-TEM), we investigate the concentration dependence of cluster size through independent approaches. We then propose a simple dissolution model grounded in basic thermodynamics to explain the observed increasing trend.

2 Experimental

2.1 Materials

As_2S_3 solutions were prepared by dissolving amorphous As_2S_3 powder (Alfa Aesar 99.999%) in *n*-propylamine (Sigma-Aldrich 99.9%) at ten concentrations: 0.01, 0.04, 0.07, 0.1, 0.2, 0.3, 0.4, 0.7, 0.8, and 1.0 moles per liter solvent (mol L_{solv}^{-1}). Subsets of these concentrations were used for each kind of measurement, depending on restrictions of the technique. Solutions were prepared in a nitrogen atmosphere glovebox to avoid oxidation and humidity. Each was left for a week to dissolve and passed through a 0.1 μm millipore filter prior to characterization.

Department of Mechanical and Aerospace Engineering, Princeton Institute for the Science and Technology of Materials, Princeton University, Princeton, New Jersey 08544, USA. E-mail: cbarnold@princeton.edu

2.2 Room temperature measurements

Samples for DLS were sealed in an optical glass cuvette with a polytetrafluoroethylene stopper, and measurements were performed using a Malvern Zetasizer Nano with backscatter detector and a 633 nm laser. Approximate measurements of relative kinematic viscosity were performed by timing solutions as they flowed through a segment of a capillary tube and comparing to the time taken by the pure solvent. These values were converted to relative dynamic viscosities using the known density of each solution.

2.3 Cryo-electron microscopy

Samples for cryo-TEM were prepared using an FEI Vitrobot. Solution was deposited on a 200 mesh copper grid with a Quantifoil substrate and 1.2 μm holes. The sample was blotted before being plunged into liquid nitrogen. Nitrogen was used *in lieu* of the normal liquid ethane bath to avoid dissolving the organic solvent, as per Oostergetel *et al.*[25] Micrographs were acquired on a Thermo Scientific Titan Krios G3 with Volta Phase Plate, operated at 300 kV and 165k× magnification.

Concentrated solutions blotted poorly in the Vitrobot, while highly dilute solutions showed little to no features during imaging. Thus, the mid-range concentrations 0.2, 0.3, and 0.4 mol L_{solv}^{-1} were used for the cryo-TEM analysis. Distributions of cluster sizes were measured in ImageJ on micrographs taken at similar levels of defocus.[26] The *z*-average size was computed for easier comparison to DLS using the formula:

$$\overline{d_z} = \frac{\sum_i n_i d_i^6}{\sum_i n_i d_i^5} \quad (1)$$

This conversion was successfully employed in a similar study by Tuoriniemi *et al.*[27]

3 Results and discussion

The *z*-average sizes of As_2S_3 clusters in *n*-propylamine determined by DLS are shown in Fig. 1, alongside similar data from Lu *et al.*[13] Data from Kohoutek *et al.* for $As_{33}S_{67}$ in *n*-butylamine is presented as well for qualitative comparison.[21] All experiments show a concentration-dependent increase in cluster size with consistent slope, even as we have expanded the range explored in the previous studies.

Interpreting this trend requires that we first consider any experimental artifacts that may affect its validity. In DLS, such artifacts can arise from the fact that the cluster size is not directly measured, but rather is calculated from the measured diffusion coefficient using the Stokes–Einstein equation:

$$D = \frac{k_B T}{6\pi\eta R_H} \quad (2)$$

where η is the viscosity of the pure solvent. Because of this, a viscosity increase with concentration can lead to restricted diffusion and an artificially large apparent cluster size.

To check if viscosity increases are responsible for the observed trend, the viscosity of the solution relative to that of the pure solvent was measured over a range of concentrations. The data, shown in Fig. 2, is consistent with results from Song.[28] While there is a clear viscosity increase with concentration, it is not steep enough to fully explain the trend observed in Fig. 1.

Size measurements were also taken in cryo-TEM—a direct technique not affected by viscosity changes—as a separate verification in the range of concentrations where it was feasible. An example micrograph is shown in the inset of Fig. 1. Results of the size measurements, shown by the red square markers in Fig. 1, were consistent with DLS. This further establishes that the observed trend is not purely a DLS artifact.

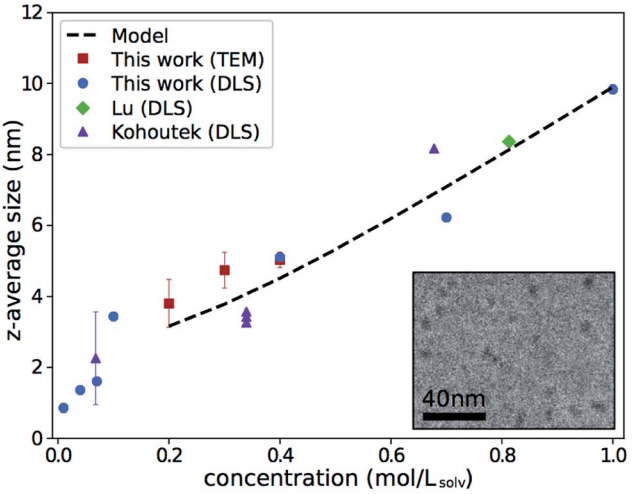

Fig. 1 *Z*-average size of As_2S_3 clusters in amines. Results from this work, Lu are for As_2S_3 in *n*-propylamine; results from Kohoutek are for $As_{33}S_{67}$ in *n*-butylamine, and only values acquired with a 632.8 nm laser are shown.[13,21] Error bars for this work show the standard deviation of repeat measurements and are often smaller than the marker. Inset shows an example cryo-TEM micrograph of 0.3 mol L_{solv}^{-1} solution. Electron-dense As_2S_3 clusters appear as dark spots on *n*-propylamine background.

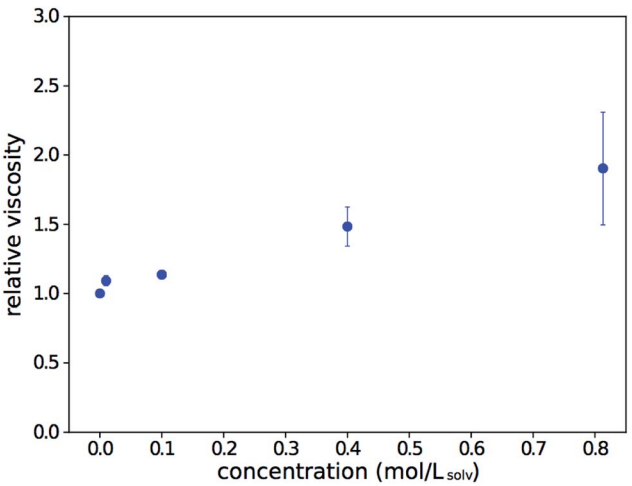

Fig. 2 Relative dynamic viscosity of As_2S_3 solutions in *n*-propylamine, compared to that of the pure solvent. Error bars show the standard error of repeat measurements.

3.1 Dissolution analysis

Previous efforts to describe the dissolution of As–S compounds in amines have focused on the mechanism of chemical interaction between the solvent and solute.[20,29] While these proposals explain some of the process, they are not sufficient to understand why cluster size should vary for different concentrations of the same composition of glass. Thus, to explain our results, we take a different approach and consider As_2S_3 cluster formation as a question of thermodynamics.

To begin, we propose a simplified dissolution model where the process occurs in two steps: (1) a chemical reaction between *n*-propylamine solvent and As_2S_3 solute produces the amine salt detected by Chern *et al.* and (2) the amine salt and unreacted solute minimize surface energy by forming micelle-like clusters.[20] This process is illustrated in Fig. 3 and is highly general, leaving room for the subsequent calculations to be applied to similar systems.

Within this model, the average cluster size at a given concentration must depend on the ratio of amine salt to unreacted As_2S_3. We can calculate this by considering the governing chemical reaction of the system:[12]

$$As_2S_3 + 6C_3H_7NH_2 \rightarrow (C_3H_7NH_3)_3AsS_3 + (C_3H_7NH)_3As \quad (3)$$

In our calculation, we will denote the reactants As_2S_3 and *n*-propylamine by the subscripts A and B, respectively. The product $(C_3H_7NH_3)_3AsS_3$ is the amine salt, which we will denote by the subscript C. The product $(C_3H_7NH)_3As$ is a precipitate, which previous work has shown can be filtered out to leave As voids in deposited films;[30] we will denote it by the subscript D.

After ξ moles of As_2S_3 have reacted, the number of moles of a component i is given by:

$$n_i = n_{i,0} + \nu_i\xi \quad (4)$$

where $n_{i,0}$ is the initial moles of the component and ν_i is its stoichiometric coefficient—negative for reactants and positive for products. The Gibbs free energy of the system at this point can thus be written:

$$\begin{aligned} G &= \sum_i \mu_i n_i \\ &= \sum_i \mu_i (n_{i,0} + \nu_i\xi) \end{aligned} \quad (5)$$

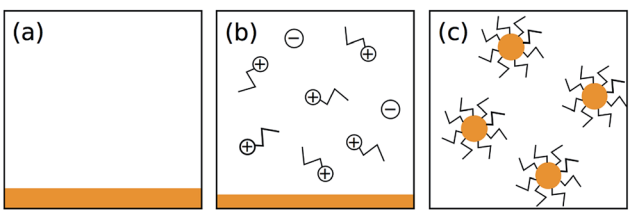

Fig. 3 Illustration of proposed dissolution model: (a) initial state of the system with unreacted As_2S_3 (orange sediment) and *n*-propylamine (white background), (b) state of the system after reaction has proceeded to equilibrium with amine salt ions in solution and unreacted As_2S_3 remaining (precipitating reaction product not shown), and (c) final state of the system after amine salt and unreacted As_2S_3 have organized into energetically favorable structure.

where μ_i is the chemical potential of component i. We can rewrite μ_i in terms of the free energy of formation G_i^0 and activity a_i to get:

$$\begin{aligned} G &= \sum_i (G_i^0 + R_gT \ln a_i)(n_{i,0} + \nu_i\xi) \\ &= \sum_i n_{i,0}G_i^0 + \xi\sum_i \nu_i G_i^0 + R_gT\sum_i (n_{i,0} + \nu_i\xi)\ln a_i \end{aligned} \quad (6)$$

Finally, we note that $\sum \nu_i G_i^0$ is simply the steady-state free energy of reaction, ΔG_R^0. This gives the final generalized result:

$$G = \sum_i n_{i,0}G_i^0 + \xi\Delta G_R^0 + R_gT\sum_i (n_{i,0} + \nu_i\xi)\ln a_i \quad (7)$$

We can now apply eqn (7) to the As_2S_3 and *n*-propylamine system. For a solution mixed at concentration c mol L_{solv}^{-1}, there are c starting moles of As_2S_3 ($n_{A,0} = c$ mol) and approximately 12 starting moles of *n*-propylamine ($n_{B,0} = 12$ mol) that react as described in eqn (3). Inserting this into eqn (7) gives:

$$\begin{aligned} G = cG_A^0 + (12\text{ mol})G_B^0 + \xi\Delta G_R^0 + R_gT[(c-\xi)\ln a_A + (12\text{ mol} - 6\xi) \\ \ln a_B + \xi(\ln a_C + \ln a_D)] \end{aligned} \quad (8)$$

Assuming that pure solids and liquids are in their standard states, we can set the activities of components A, B, and D to unity to get the simplified result:

$$G = cG_A^0 + (12\text{ mol})G_B^0 + \xi\Delta G_R^0 + R_gT\xi \ln a_C \quad (9)$$

For a sufficiently dilute solution, we can approximate the activity a_C of component C as its molarity. This is given by the moles of component C divided by the combined volume of component C and the solvent; components A and D are not dissolved, so their volumes do not contribute. Inspecting eqn (3) shows that approximately half of the reacted solvent volume goes into component C, so we can use the solvent density ρ_B and molecular weight MW_B to approximate the solution volume:

$$V_{soln} = (12\text{ mol} - 6\xi + 3\xi)\frac{MW_B}{\rho_B} \quad (10)$$

Using this to write the molarity of component C and inserting into eqn (9) yields the final result for the Gibbs free energy of the system:

$$G = cG_A^0 + (12\text{ mol})G_B^0 + \xi\Delta G_R^0 + R_gT\xi \ln\left[\frac{\xi\rho_B}{(12\text{ mol} - 3\xi)MW_B}\right] \quad (11)$$

It is clear from eqn (11) that the Gibbs free energy increases with concentration; this makes sense, since we have not written G in per molar form. However, since c and ξ never appear in the same term of the Gibbs function, the derivative $\frac{\delta G}{\delta \xi}$ must not have a c dependence. This means the equilibrium extent of reaction—the value ξ_{eq} that minimizes G—is independent of solution concentration, depending only on material constants and temperature.

To relate this conclusion to the average As_2S_3 cluster size at varying concentrations, we make three geometric assumptions:

(1) The clusters are approximately spherical. This is supported by our cryo-TEM micrographs; the clusters pictured in the inset of Fig. 1 are generally round in shape.

(2) The clusters follow the form proposed by Chern *et al.*—an amine salt on the surface and as-bulk As_2S_3 within the volume—the justification for which is well explained in their original work.[20]

(3) Each molecule contributes either a characteristic volume or characteristic surface area to the cluster it is part of. This assumes a uniform solid density, reasonable in the absence of external forces.

Following these assumptions, we will use the terms V_A (volume contributed by an As_2S_3 molecule) and SA_C (surface area contributed by a $(C_3H_7NH_3)_3AsS_3$ molecule) to proceed with the calculation.

If we mix c mol of As_2S_3 and 1 L of solvent, the number of clusters at equilibrium can be written in two ways. The first is found by dividing the total volume of As_2S_3 available for cluster formation by the volume of an individual cluster:

$$n = \frac{(cV_A - \xi_{eq}V_{As})N_A}{\frac{4}{3}\pi R^3} \quad (12)$$

Note that $\xi_{eq}V_{As}$ represents the volume of arsenic that precipitates out during the reaction and is therefore not available to form clusters. Note also that the subscript in N_A does not refer to component A, but rather to Avogadro's constant.

The second expression for n is found by dividing the total surface area available for cluster formation by the surface area of an individual cluster:

$$n = \frac{\xi_{eq}SA_CN_A}{4\pi R^2} \quad (13)$$

We can now equate eqn (12) and (13):

$$\frac{(cV_A - \xi_{eq}V_{As})N_A}{\frac{4}{3}\pi R^3} = \frac{\xi_{eq}SA_CN_A}{4\pi R^2} \quad (14)$$

And simplify to relate R, c, and ξ_{eq}:

$$R[c, \xi_{eq}] = \left(\frac{3V_A}{\xi_{eq}SA_C}\right)c - \frac{3V_{As}}{SA_C} \quad (15)$$

Since ξ_{eq} is independent of c, eqn (15) shows a linear relationship between cluster size and solution concentration. The slope, $\frac{3V_A}{\xi_{eq}SA_C}$, contains only positive terms and must therefore be increasing.

By solving eqn (15) for ξ_{eq} and inserting into eqn (11) as ξ, we can obtain the Gibbs free energy of a solution where at some arbitrary ξ, the reaction halts and clusters form. This allows us to plot the free energy against the cluster size that results from each ξ. The predicted cluster size, which corresponds to the true ξ_{eq}, will minimize the Gibbs function. This is shown for different concentrations in Fig. 4. Each G curve is scaled to account for the cG_A^0 term in eqn (11), so the curves line up vertically and can be more easily compared. With this view, it is clear that the predicted cluster size increases with concentration.

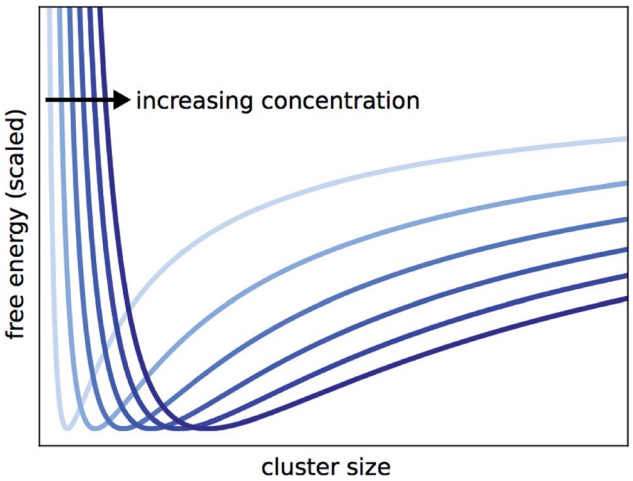

Fig. 4 Scaled Gibbs free energy of solution *versus* cluster size; concentration increases with line darkness. The scaling removes the linear increase in G with c, so plots are leveled for an easier comparison of overall shape. The predicted average cluster size is that which minimizes G.

To attain z-averages from the model for comparison with experiments, the average cluster size was calculated from eqn (15) and used to generate a normal distribution of sizes with the standard deviation observed in cryo-TEM. The z-averages were then calculated using eqn (1). The true ξ_{eq} for the system could not be calculated without ΔG_R^0, so ΔG_R^0 was used as a parameter to fit the results of the model to our experimental data.

The results of these calculations are shown by the dashed line in Fig. 1. The values correspond to $\Delta G_R^0 = -16.2$ kJ mol^{-1}. The fact that ΔG_R^0 is negative implies an exothermic reaction, in line with the fact that the dissolution happens spontaneously. However, the magnitude of ΔG_R^0 is relatively low, suggesting it is only energetically favorable to produce a small amount of product. This is consistent with Chern *et al.*'s observation that optical properties of concentrated solutions stay similar to those of bulk As_2S_3.[20] Thus, the value is in line with expectations, indicating a reasonable fit.

Note that the dashed line in Fig. 1 is limited to concentrations $\geq$0.2 mol L_{solv}^{-1}. This is because the dissolution model assumes the initial moles of $As_2S_3 \geq \xi_{eq}$, and $\xi_{eq} \approx 0.2$ mol for 1 L solvent for the calculation plotted. A different approach must be taken for concentrations below this limit, which is beyond the scope of the present work. Nevertheless, in the region for which the model is applicable, the calculations show good trend agreement with experiments.

4 Conclusions

The size of As_2S_3 clusters in amine solution and its dependence on concentration has been explored. We established the increase of cluster size with solution concentration over a larger range than had been considered in previous work. By combining DLS with viscosity measurements and cryo-TEM, we

addressed the possibility that this trend was an experimental artifact.

To explain these results, we proposed a simplified dissolution model consisting of a chemical reaction step and a structuring step; the observed concentration dependence then followed from solution thermodynamics. This approach was highly general and can be applied to other systems where dissolution is controlled by a reaction similar to eqn (3). Our calculations showed good trend agreement with experiments and together present a method for informed size control of As_2S_3 clusters that will enable improved property control in solution processing and optoelectronic device fabrication.

Conflicts of interest

There are no conflicts to declare.

Acknowledgements

The authors thank Leon Wang and Robert Prud'homme for use of and assistance with their DLS setup. The authors also thank Paul Shao, John Schreiber, and Nan Yao for many hours of support with the cryo-TEM. This research was supported by NSF through Princeton University's Materials Research Science and Engineering Center (DMR-1420541).

Notes and references

1 B. J. Eggleton, B. Luther-Davies and K. Richardson, *Nat. Photonics*, 2011, **5**, 141–148.
2 C. Tsay, E. Mujagic, C. K. Madsen, C. F. Gmachl and C. B. Arnold, *Opt. Express*, 2010, **18**, 15523–15530.
3 T. Kanamori, Y. Terunuma, S. Takahashi and T. Miyashita, *J. Lightwave Technol.*, 1984, **2**, 607–613.
4 J. S. Sanghera and I. D. Aggarwal, *J. Non-Cryst. Solids*, 1999, **256–257**, 6–16.
5 J. S. Sanghera, C. M. Florea, L. B. Shaw, P. Pureza, V. Q. Nguyen, M. Bashkansky, Z. Dutton and I. D. Aggarwal, *J. Non-Cryst. Solids*, 2008, **354**, 462–467.
6 K. Petkov and P. J. S. Ewen, *J. Non-Cryst. Solids*, 1999, **249**, 150–159.
7 A. E. Owen, A. P. Firth and P. J. S. Ewen, *Philos. Mag. B*, 1985, **52**, 347–356.
8 J. M. Harbold, F. O. Ilday, F. W. Wise, J. S. Sanghera, V. Q. Nguyen, L. B. Shaw and I. D. Aggarwal, *Opt. Lett.*, 2002, **27**, 119–121.
9 J. Teteris and M. Reinfelde, *J. Non-Cryst. Solids*, 2003, **326–327**, 494–499.
10 M. Frumar and T. Wagner, *Curr. Opin. Solid State Mater. Sci.*, 2003, **7**, 117–126.
11 A. Lepicard, F. Adamietz, V. Rodriguez, K. Richardson and M. Dussauze, *Opt. Mater. Express*, 2018, **8**, 1613–1624.
12 Y. Zha, M. Waldmann and C. B. Arnold, *Opt. Mater. Express*, 2013, **3**, 1259–1272.
13 C. Lu, J. M. P. Almeida, N. Yao and C. Arnold, *Appl. Phys. Lett.*, 2014, **105**, 1–4.
14 E. A. Sanchez, M. Waldmann and C. B. Arnold, *Appl. Opt.*, 2011, **50**, 1974–1978.
15 S. Novak, P. T. Lin, C. Li, C. Lumdee, J. Hu, A. Agarwal, P. G. Kik, W. Deng and K. Richardson, *ACS Appl. Mater. Interfaces*, 2017, **9**, 26990–26995.
16 Y. Zha, P.-T. Lin, L. Kimerling, A. Agarwal and C. B. Arnold, *ACS Photonics*, 2014, **1**, 153–157.
17 Y. Zou, L. Moreel, H. Lin, J. Zhou, L. Li, S. Danto, J. D. Musgraves, E. Koontz, K. Richardson, K. D. Dobson, R. Birkmire and J. Hu, *Adv. Opt. Mater.*, 2014, **2**, 759–764.
18 T. Kohoutek, J. Orava, T. Sawada and H. Fudouzi, *J. Colloid Interface Sci.*, 2011, **353**, 454–458.
19 C. Markos, S. N. Yannopoulos and K. Vlachos, *Opt. Express*, 2012, **20**, 14814–14824.
20 G. C. Chern and I. Lauks, *J. Appl. Phys.*, 1983, **54**, 2701–2705.
21 T. Kohoutek, T. Wagner, M. Frumar, A. Chrissanthopoulos, O. Kostadinova and S. N. Yannopoulos, *J. Appl. Phys.*, 2008, **103**, 1–6.
22 R. Tintu, V. P. N. Nampoori, R. Radhakrishnan, N. V. Unnikrishnan and S. Thomas, *J. Optoelectron. Adv. Mater.*, 2012, **14**, 918–922.
23 M. Waldmann, J. D. Musgraves, K. Richardson and C. B. Arnold, *J. Mater. Chem.*, 2012, **22**, 17848–17852.
24 J. Wang, M. Lin, T. Zhang, Y. Yan, P. C. Ho, Q.-H. Xu and K. P. Loh, *J. Am. Chem. Soc.*, 2008, **130**, 11596–11597.
25 G. T. Oostergetel, F. J. Esselink and G. Hadziioannou, *Langmuir*, 1995, **11**, 3721–3724.
26 C. A. Schneider, W. S. Rasband and K. W. Eliceiri, *Nat. Methods*, 2012, **9**, 671–675.
27 J. Tuoriniemi, A.-C. J. H. Johnsson, J. P. Holmberg, S. Gustafsson, J. A. Gallego-Urrea, E. Olsson, J. B. C. Pettersson and M. Hassellov, *Sci. Technol. Adv. Mater.*, 2013, **15**, 035009.
28 S. Song, Ph.D. thesis, Princeton University, 2011.
29 S. Slang, K. Palka, L. Loghina, A. Kovalskiy, H. Jain and M. Vlcek, *J. Non-Cryst. Solids*, 2015, **426**, 125–131.
30 Y. Zha, S. Fingerman, S. J. Cantrell and C. B. Arnold, *J. Non-Cryst. Solids*, 2013, **369**, 11–16.